ORIGINAL ARTICLE

Design, synthesis, and biological evaluation of diarylpyrazole derivatives as antitumor agents targeting microtubules

Jing Chang [a,b,1], Chao Wang [b,*,1], Shanbo Yang [a,b], Lingyu Shi [a,b], Yujing Zhang [c], Wenjing Liu [a,b], Jingsen Meng [a,b], Jun Zeng [a,b], Renshuai Zhang [b], Ning Liu [b,*], Dongming Xing [b,d,*]

[a] School of Basic Medicine, Qingdao University, Qingdao 266071, Shandong, China
[b] The Affiliated Hospital of Qingdao University, Cancer Institute, Qingdao University, Qingdao 266071, Shandong, China
[c] The Affiliated Cardiovascular Hospital of Qingdao University, Qingdao University, Qingdao 266071, Shandong, China
[d] School of Life Sciences, Tsinghua University, Beijing 100084, China

Abstract   A new series of novel diarylpyrazole derivatives as microtubule destabilizers were synthesized and evaluated for the anti-proliferative activities. Anti-proliferative assays were performed on the human cervix adenocarcinoma cell line (HeLa) and human gastric adenocarcinoma cell line (SGC-7901), and the compound **9s** containing indole ring showed great anti-proliferative activity against HeLa cells with IC$_{50}$ value of 1.9 $\pm$ 0.11 μM. Further biological studies showed that **9s** was able to inhibit tubulin polymerization, disrupt the cytoskeleton, block the cell cycle in the G2/M phase, and induce cell apoptosis in a concentration-dependent manner. In addition, the results of molecular docking studies showed that compound **9s** could bind tightly to the colchicine binding site of tubulin through hydrogen bonding interaction. These preliminary results recommend that compound **9s** is likely to be a microtubule destabilizer that deserves further investigation.

* Corresponding authors at: The Affiliated Hospital of Qingdao University, Cancer Institute, Qingdao University, Qingdao 266071, Shandong, China (D. Xing).
   E-mail addresses: wangchao20086925@126.com (C. Wang), leirum_ln@qdu.edu.cn (N. Liu), xdm_tsinghua@163.com (D. Xing).
[1] Share the first author.

1. Introduction

Microtubules are cylindrical polymers composed of microtubule protein subunits α and β, which are highly dynamic cytoskeletal fibers and key structural components of eukaryotic cells (Wang et al., 2019; Wang et al., 2020). Microtubules play an important role in cellular functions such as cell division and mitotic spindle formation, cell shape maintenance, and cell viability (Jordan and Wilson, 2004; Wang et al., 2021). Therefore, microtubules have long been considered attractive targets for clinically effective anticancer drugs, the discovery and development of small molecules which target on tubulin to hamper

the dynamic of tubulin polymerization has been an established strategy for anticancer therapy (Attard et al., 2006; Loong and Yeo, 2014). Microtubule-targeting drugs can be classified into two types according to the different ways of disrupting microtubule dynamics. The former is microtubule stabilizers such as paclitaxel and epothilone and the latter is microtubule destabilizers such as colchicine (1, Fig. 1), combretastatin A-4 (CA-4, 2, Fig. 1) (Cao et al., 2018). While there are no clinically approved microtubule destabilizers (Wang et al., 2022), a number of effective microtubule destabilizers are currently being investigated in clinical studies.

CA-4, a natural chain alkane isolated by Pettit from the African willow *Combretum caffrum*, was found to be a potent anti-mitotic drug that inhibits microtubule protein polymerization and the binding of colchicine to microtubulin (Lin et al., 1989; Wang et al., 2021). Due to its highly unstable *cis*-olefin, the A and B rings change from *cis* to *trans* in the presence of light and heat, leading to the loss of biological activity (Greene et al., 2010). Therefore, stabilization of the *cis*-olefin in the structure of CA-4 is a major trend. In recent years, it has been the pursuit of major researchers to use the heterocyclic ring to replace the *cis*-olefin in CA-4 structure with CA-4 as a lead compound, and to make the A ring and B ring in *cis* structure at the same time (Siebert et al., 2016). In the past, pyrazole (3, 4, 5, Fig. 1) (Johnson et al., 2007; Wang et al., 2019), furazan (6, Fig. 1) (Tron et al., 2005), tetrazole (7, Fig. 1) (Beale et al., 2012), and pyridine (8, Fig. 1) (Zheng et al., 2014), have been used to replace the *cis*-olefin structure of CA-4 with desirable results.

Pyrazole, as a pharmacologically important active scaffold, is one of the most studied moieties among the azoles, and it is also an important class of five-membered heterocyclic compounds with almost all types of pharmacological activities, such as anti-inflammatory, antitumor, and antidepressant activities (Hannah et al., 1975; Abdel-Aziz et al., 2009; Kucukguzel and Senkardes, 2015). Bioisosterism plays a major role in the search for analogues of an active drug molecule (Lima and Barreiro, 2005). Application of bioisosterism instead of the *cis*-olefin on the structure of CA-4 is one of the strategies often used in the design of the CA-4 analogues. The modification of *cis*-olefin has led to varied cytotoxic activity.

As a part of our continuing effort on the development of novel antitumor agents, we designed a series of novel CA-4 analogues (9, Fig. 2) by introducing a pyrazole, hydrogen-bonding acceptors, as *cis*-olefin of CA-4. Herein, we described the detailed synthetic routes,

anti-proliferative, tubulin polymerization, immunofluorescence staining analysis, cell cycle analysis, and cell apoptosis analysis of these compounds.

2. Result and discussion

2.1. Chemistry

The synthetic route for the target compounds (9a-9t) is outlined in Scheme 1. The key intermediate 4-bromo-1-(3,4,5-tri methoxyphenyl)-1*H*-pyrazole (11) was prepared by using 4-bromo-1*H*-pyrazole (10) as the starting material (Kumar et al., 2019). Subsequently, the target compounds (9a-9t) were obtained by treating compound 11 with phenylboronic acid, Pd(PPh₃)₄, and K₂CO₃ *via* Suzuki crosscoupling reaction (Li et al., 2020; Yang et al., 2020).

2.2. Biological evaluation

2.2.1. In vitro anti-proliferative activity

All of the target compounds, 9a-9t, along with the positive control, CA-4 (2), were evaluated for their anti-proliferative activity against two human cancer cell lines: human cervical cancer cells HeLa, gastric adenocarcinoma cells SGC-7901. Some target compounds displayed anti-proliferative activity with IC_{50} values in the micromolar range. This indicates that the pyrazole moiety is suitable for mimicking the *cis*-olefin moiety in CA-4, as analogues with the pyrazole moiety maintain potent anti-proliferative activities against multiple cancer cell lines.

As illustrated in Table 1, some target compounds showed moderate anti-proliferative activities with potencies in the micromolar range. In general, the strongest anti-proliferative activity against the two cell lines with IC_{50} value of 1.9--3.2 μM was observed when the B ring was substituted with indole ring (9s), while a sharp decrease in anti-proliferative activity was observed when the B ring was
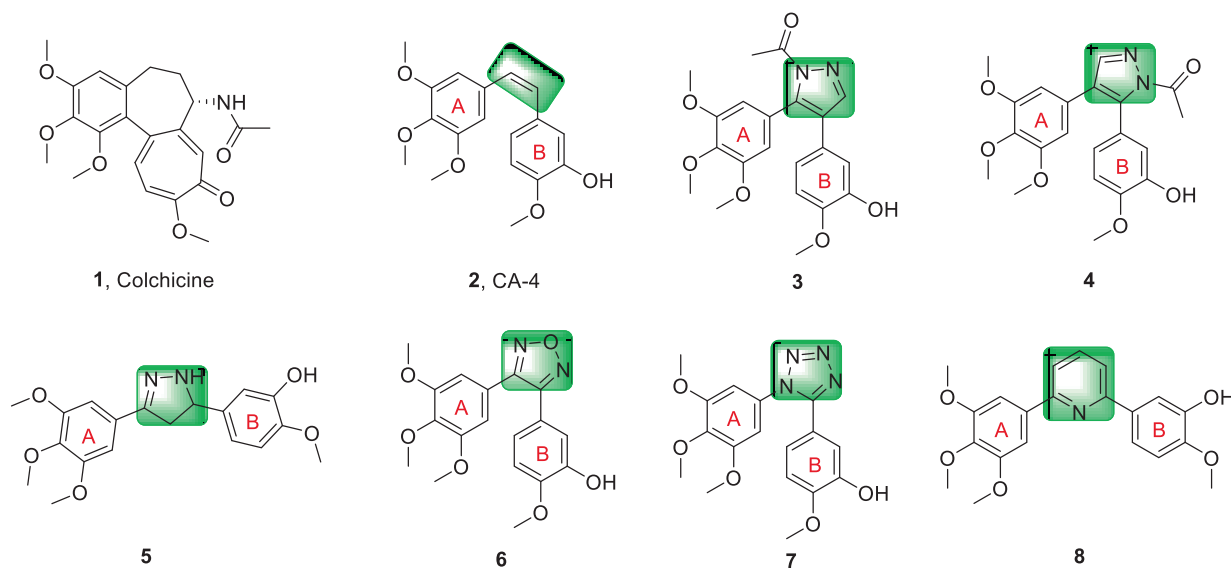

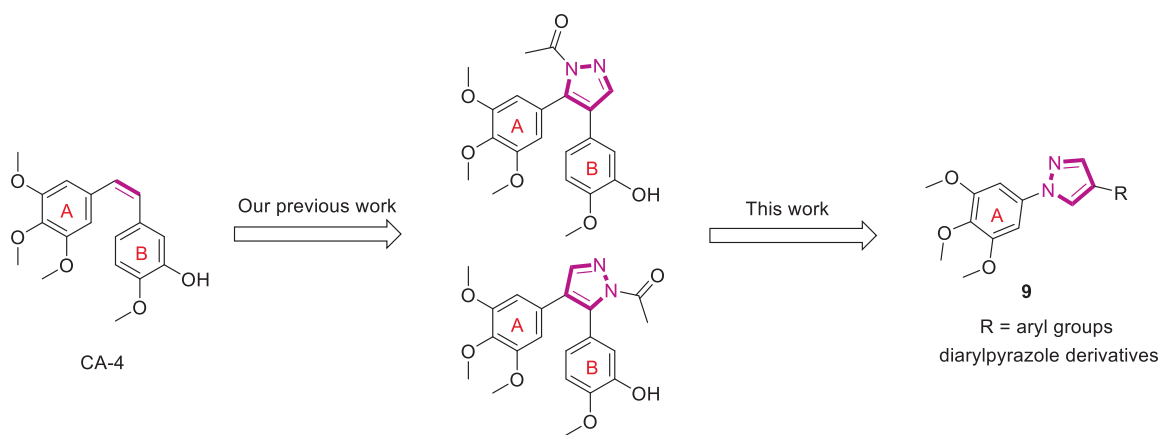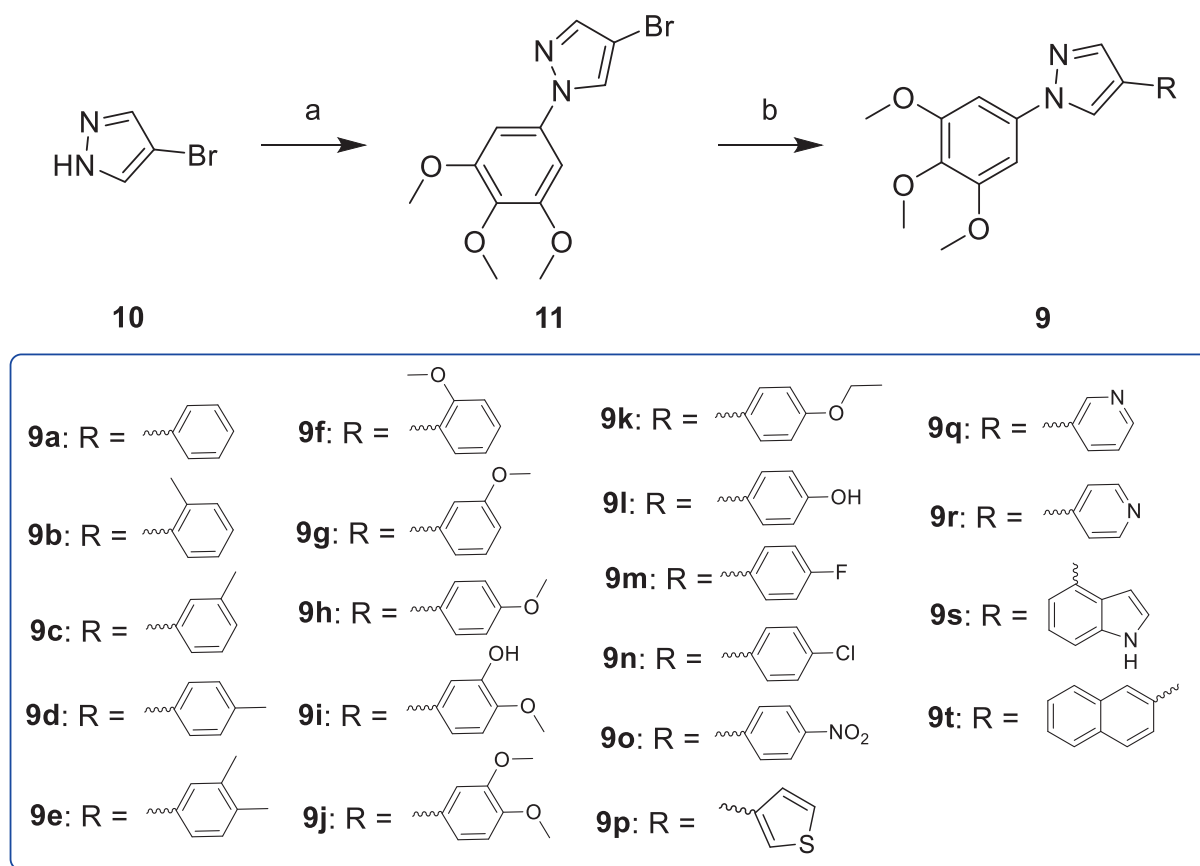**Fig. 1** Chemical structures of some microtubule destabilizers.

Fig. 2 The design of target compounds.

Scheme 1 Reagents and conditions: (a) 3,4,5-trimethoxyphenylboronic acid, Cu(OAc)$_2$, pyridine, DCM, r.t.; (b) Substituted phenylboronic acid, Pd(PPh$_3$)$_4$, K$_2$CO$_3$, 1,4-dioxane/H$_2$O = 3/1, N$_2$ atmosphere, 126 °C, M.W. irradiation.

substituted with other aryl/heteroaryl groups, such as thiophene (**9p**), pyridine (**9r**) and naphthalene (**9t**). Comparison of the IC$_{50}$ values of the corresponding compounds **9a-9o** with benzene or substituted benzene revealed that compounds **9a**, **9h**, **9i**, and **9l** significantly inhibited the growth of the HeLa and SGC-7901 cell lines at 10 μM. The target compounds contain halide and nitro substituents that have been widely used by medicinal chemists in microtubule destabilizers research, so we synthesize these compounds to evaluate the potential anti-proliferative activities. Unexpectedly, we found that these compounds (**9m**, **9n**, and **9o**) showed weak anti-proliferative activities.

Table 1 Anti-proliferative activity of all compounds.

Compounds	(IC$_{50}$ ± SD, μM)	
	HeLa	SGC-7901
9a	10.2 ± 1.2	13.6 ± 1.7
9b	30.6 ± 3.7	39.3 ± 4.0
9c	22.8 ± 2.3	25.2 ± 2.9
9d	17.2 ± 1.4	15.6 ± 1.7
9e	27.6 ± 3.3	> 50
9f	32.8 ± 3.7	> 50
9g	18.8 ± 2.0	16.9 ± 1.9
9h	8.1 ± 0.6	9.8 ± 0.9
9i	10.1 ± 1.3	12.3 ± 1.2
9j	30.6 ± 3.5	> 50
9k	> 50	32.6 ± 3.6
9l	10.8 ± 1.9	16.0 ± 2.3
9m	35.2 ± 4.2	40.6 ± 3.7
9n	> 50	> 50
9o	> 50	> 50
9p	> 50	40.3 ± 5.2
9q	> 50	> 50
9r	33.2 ± 4.5	31.2 ± 3.6
9s	**1.9 ± 0.11**	**3.2 ± 0.39**
9t	35.8 ± 4.3	27.2 ± 3.2
CA-4	0.078 ± 0.008	0.096 ± 0.011

IC$_{50}$: the half maximal inhibitory concentration.
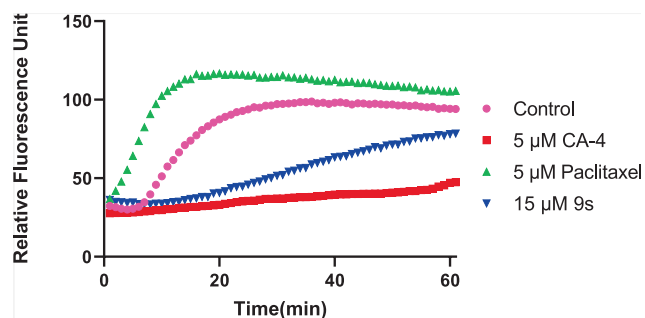CA-4: used as positive controls.

Fig. 3 Effects of compound **9s** on tubulin polymerization. Tubulin had been pre-incubated for 1 min with **9s** at 15 μM, 5 μM of CA-4, Paclitaxel at 5 μM or vehicle DMSO at room temperature before GTP was added to start the tubulin polymerization reactions. The reaction was monitored at 37 °C.

2.2.2. Effect on tubulin polymerization

To explore the anti-proliferative activity of these compounds in relation to microtubulin, the most active compound **9s**, was evaluated for its effect on microtubulin polymerization and compared with the positive control CA-4 and the negative control paclitaxel. As shown in Fig. 3, both CA-4 and compound **9s** inhibited microtubulin polymerization. In contrast, paclitaxel increased the rate of microtubulin polymerization. These results indicate that compound **9s** has an interfering effect on microtubulin polymerization.
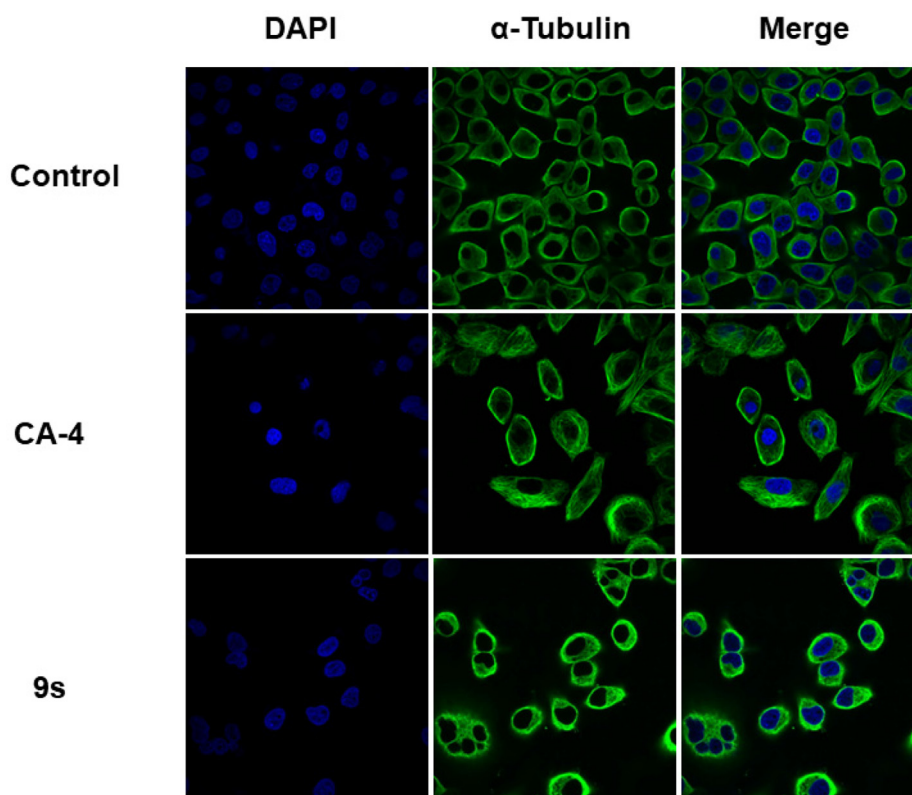

Fig. 4 Effects of compound **9s** and CA-4, at their respective 2-fold IC$_{50}$ concentrations, on the cellular microtubule network and microtubule reassemble by immunofluorescence. HeLa cells were treated with compound **9s** or CA-4 for 24 h, and then direct microscopy detection of the fixed and stained cell was performed. Microtubules and unassembled microtubule proteins were stained with anti-a-tubulin-FITC specific antibodies (green). Nuclei were stained by 4′,6-diamidino-2-phenylindole (DAPI, blue).

2.2.3. Analysis of immunofluorescence staining

To clarify the mechanism of action of compound **9s**, immunofluorescence staining was performed to further evaluate the effect of compound **9s** on microtubule protein assembly. HeLa cells were treated with CA-4 and compound **9s** at their respective 2-fold IC_{50} concentrations for 24 h. As shown in Fig. 4, the cells treated with compound **9s** showed changes in the shape of the nucleus, and the microtubule network became disorganized and shrunken or even appeared multinucleated compared with the control group. These results demonstrate that the mechanism of action of compound **9s** is similar to that of CA-4 in that both inhibit microtubule assembly and disrupt the cytoskeleton.

2.2.4. Cell cycle analysis

As we all know, tubulin inhibitors arrest cell cycle distribution in G2/M phase (Wu et al., 2017). To explore the possible antitumor mechanisms of diarylpyrazole derivatives, the most promising compound **9s**, was selected and its effect on HeLa cell cycle progression was analyzed by flow cytometry. In the present work, HeLa cells were treated with **9s** at concentrations of 2-fold IC_{50}, 5-fold IC_{50}, and 10-fold IC_{50} and control for 24 h, respectively. As shown in Fig. 5, the percentage of cells in the G2/M phase of the cell cycle increased from

18.17% to 50.63% under the treatment with the indicated concentration of **9s**, compared to 5.48% in the control. The results show that the compound **9s** caused a significant G2/M phase block in a concentration-dependent manner, which is typical for inhibitors of microtubule protein polymerization.

2.2.5. Cell apoptosis assay

The apoptosis-inducing potential of **9s**, the most cytotoxic compound, on HeLa cells was evaluated using Annexin V-FITC/PI. Examination of flow cytometry data allowed to distinguish between apoptotic (early and late) and necrotic cell populations. Compound **9s** induced apoptosis in HeLa cells already at its IC_{50} concentration, as shown in Fig. 6. The total number of early (Q3) and late (Q2) cells was 15.13%, 22.73% and 32.7% after 48 h of compound **9s** action at 1-fold IC_{50}, 2-fold IC_{50}, and 3-fold IC_{50} concentrations, respectively, compared to 7.1% in the control group. Thus, the results illustrate that compound **9s** has anti-proliferative activity by dose-dependently inducing apoptosis.

2.3. Molecular modeling

To investigate the possible binding of target compounds to the colchicine site of tubulin, **9s** was investigated by using
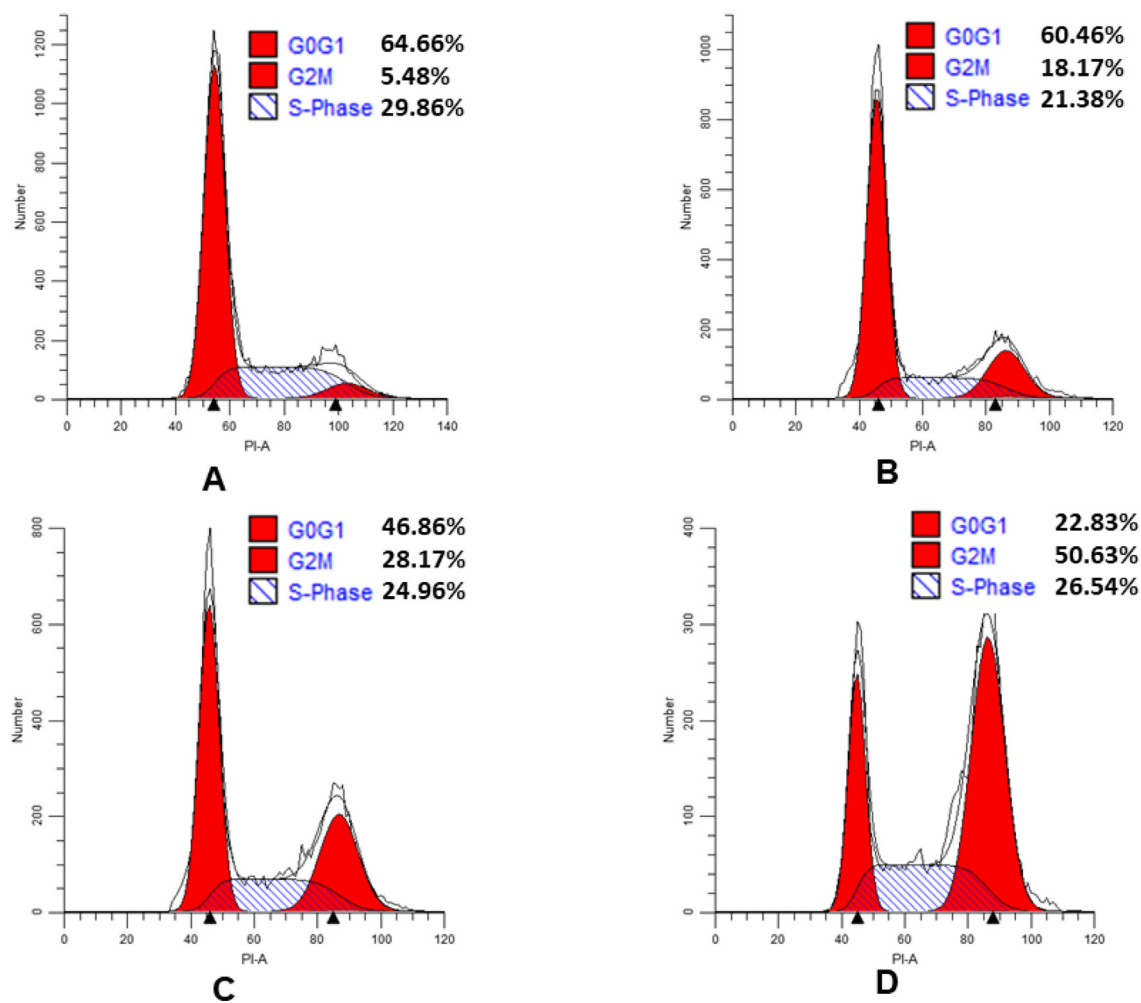

Fig. 5 Effects of compound **9s** on cell cycle. HeLa cells lines treated with compound **9s** for 24 h. (A) Control; (B) **9s**, 2-fold IC_{50}; (C) **9s**, 5-fold IC_{50}; (D) **9s**, 10-fold IC_{50}.
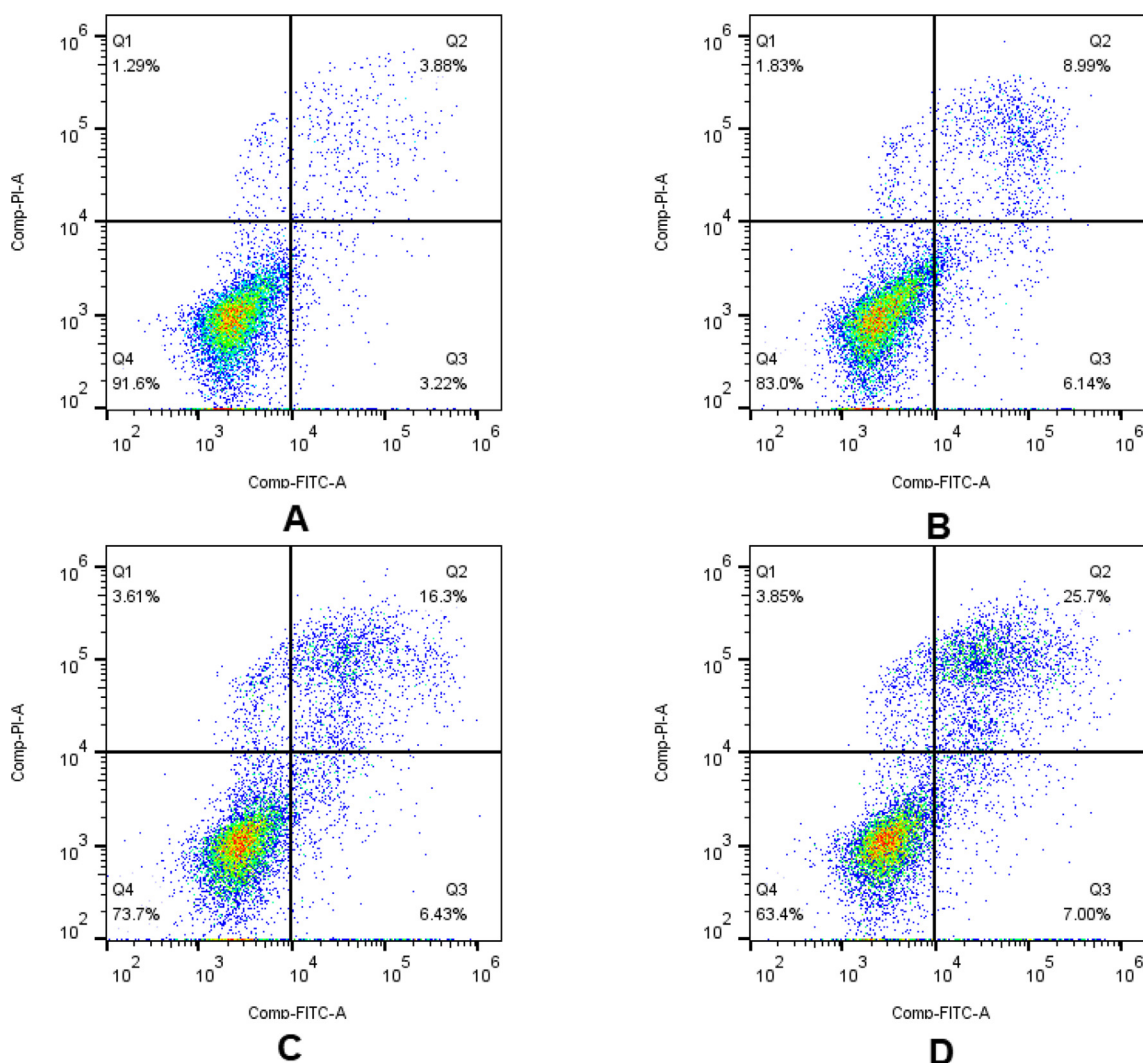
Fig. 6 Effect of compound **9s** on cell apoptosis in HeLa cells. Flow cytometric analysis of apoptotic cells after treatment of HeLa cells with **9s** or control for 48 h. (A) Control; (B) **9s**, 1-fold IC_{50}; (C) **9s**, 2-fold IC_{50}; (D) **9s**, 3-fold IC_{50}. Different cell stages were given as live (Q4), early apoptotic (Q3), late apoptotic (Q2), and necrotic cells (Q1).

CDOCKER program in Discovery Studio 3.0 software (Dorleans et al., 2009). The molecular docking simulation showed that the pose of **9s** was tightly embedded into the inter-face of α/β tubulin subunits (Fig. 7). In the binding model, the binding orientations of **9s** adopted a twisted geometry, which may be the key for its bioactivity. The oxygen atom of the
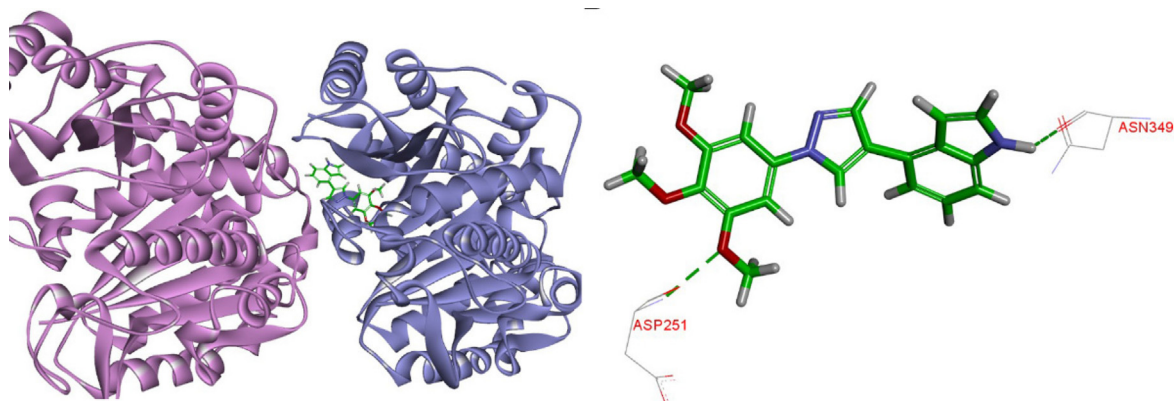

Fig. 7 (A) The binding mode of compound **9s** in the colchicine binding site of tubulin; (B) Overlay of **9s** in the binding site.

3,4,5-trimethoxy group of **9s** contributed to the hydrogen bonding interaction with the residue of βASP251. Furthermore, nitrogen atom of indole forms a hydrogen bond with the residue βASN349.The docking study was a beneficial complement and explanation to the above tubulin polymerization and immunofluorescence studies (Wang et al., 2021).

3. Conclusion

In summary, we designed and synthesized a series of novel diarylpyrazole derivatives as novel microtubule destabilizers. The antiproliferative activities of all the target compounds against two different cell lines (HeLa and SGC-7901) were studied by MTT assay. Among them, compound **9s** containing indole ring had the good antiproliferation activity on HeLa cells with IC_{50} value of $1.9 \pm 0.11 \mu$ M. In addition, tubulin polymerization inhibition experiments and immunofluorescence experiments also showed that compound **9s** effectively inhibited tubulin polymerization and destroyed the microtubule network of Hela cells. Further pharmacological mechanisms showed that **9s** could significantly arrest the cell cycle in the G2/M phase and induce apoptosis in a dose-dependent manner. The final molecular docking further confirmed that compound **9s** may be a novel microtubule destabilizer. It is worthy of further study, which provides a direction for the development of novel microtubule destabilizers.

4. Experimental

4.1. Chemistry

4.1.1. Materials and methods

All reagents and solvents we use are purchased from commercial sources. We monitored the reaction using silica gel thin layer color (TLC) at UV wavelengths (365 nm and 254 nm). At room temperature, ^1H (500 MHz) and ^{13}C NMR (125 MHz) were measured on Agilent ProPulse 500 MHz (Agilent Inc. USA) using $CDCL_3$ as the solvent. Agilent Accurate-Mass Q-TOF 6530 instrument (Agilent Inc. USA) in ESI mode was used to record high resolution mass spectrometry (HRMS). The microwave were carried out in a single mode cavity microwave synthesiser (CEM MATTHEWS, NC, USA). (Wang et al., 2021).

4.1.2. General synthetic procedures for 4-bromo-1-(3,4,5-trimethoxyphenyl)-1H-pyrazole (11)

To a round-bottom flask equipped with a magnetic stir bar, 4-bromo-1H-pyrazole (**10**) (0.20 mmol), 3,4,5-trimethoxybenzeneboronic acid (0.20 mmol), $Cu(OAc)_2$ (0.40 mmol), pyridine (0.40 mmol), and dried DCM (10.0 mL) were added. The flask was evacuated and backfilled with nitrogen. The mixture was stirred at room temperature for 4 h. After completion of the reaction, the reaction mixture was extracted with DCM (25 mL × 3). The organic layer was washed with brine and dried over Na_2SO_4. The filtrate was concentrated under reduced pressure and purified by silica gel column chromatography to give **11**.

4.1.3. General synthetic procedures for diarylpyrazole derivatives (9)

A mixture of **11** (0.10 mmol), $Pd(PPh_3)_4$ (0.01 mmol), and K_2CO_3 (0.12 mmol), and substituted phenylboronic acid (0.11 mmol) in 1,4-dioxane/H_2O (5 mL, 3:1) was degassed and purged with N_2 for about three times. The reaction mixture was stirred at irradiated in a microwave reactor for 25 min at 126 °C (indicated by TLC) under N_2 atmosphere. The reaction mixture was poured into H_2O (50 mL) and extracted with ethyl acetate (EtOAc) (80 mL × 3). The combined organics were washed with brine (10 mL × 3), dried over anhydrous Na_2SO_4, filtered and concentrated under reduced pressure to give a residue, then the residue was purified by column chromatography (petroleum ether/EtOAc = 3:1) on silica gel to afford pure product **9**.

4.1.3.1. 4-phenyl-1-(3,4,5-trimethoxyphenyl)-1H-pyrazole (9a). White solid; yield: 98%; ^1H NMR (500 MHz, CDCl₃) δ 8.10 (s, 1H), 7.98 (s, 1H), 7.57 (d, J = 8.0 Hz, 2H), 7.41 (t, J = 7.7 Hz, 2H), 7.28 (t, J = 7.4 Hz, 1H), 6.95 (s, 2H), 3.95 (s, 6H), 3.88 (s, 3H); ^{13}C NMR (125 MHz, CDCl₃) δ 153.79 (2C), 138.57, 136.82, 136.19, 131.94, 128.94 (2C), 126.89, 125.69 (2C), 124.87, 123.56, 97.12 (2C), 61.04, 56.35 (2C); HRMS calcd for $C_{18}H_{19}N_2O_3$ $[M+H]^+$ 311.1396, found 311.1396.

4.1.3.2. 4-(o-tolyl)-1-(3,4,5-trimethoxyphenyl)-1H-pyrazole (9b). White solid; yield: 90%; ^1H NMR (500 MHz, CDCl₃) δ 7.94 (s, 1H), 7.84 (s, 1H), 7.41–7.36 (m, 1H), 7.30–7.27 (m, 1H), 7.24 (dt, J = 7.3, 3.2 Hz, 2H), 6.96 (s, 2H), 3.95 (s, 6H), 3.88 (s, 3H), 2.45 (s, 3H); ^{13}C NMR (125 MHz, CDCl₃) δ 153.80 (2C), 140.70, 136.79, 136.22, 135.44, 131.58, 130.73, 129.19, 127.24, 126.07, 125.51, 124.02, 97.15 (2C), 61.03, 56.36 (2C), 21.20; HRMS calcd for $C_{19}H_{21}N_2O_3$ $[M+H]^+$ 325.1552, found 325.1551.

4.1.3.3. 4-(m-tolyl)-1-(3,4,5-trimethoxyphenyl)-1H-pyrazole (9c). White solid; yield: 95%; ^1H NMR (500 MHz, CDCl₃) δ 8.09 (s, 1H), 7.97 (s, 1H), 7.37 (d, J = 12.0 Hz, 2H), 7.29 (t, J = 7.6 Hz, 1H), 7.10 (d, J = 7.5 Hz, 1H), 6.95 (s, 2H), 3.95 (s, 6H), 3.88 (s, 3H), 2.41 (s, 3H); ^{13}C NMR (125 MHz, CDCl₃) δ 153.78 (2C), 138.62, 138.56, 136.75, 136.21, 131.83, 128.85, 127.67, 126.41, 124.94, 123.50, 122.79, 97.06 (2C), 61.04, 56.35 (2C), 21.48; HRMS calcd for $C_{19}H_{21}N_2O_3$ $[M+H]^+$ 325.1552, found 325.1549.

4.1.3.4. 4-(p-tolyl)-1-(3,4,5-trimethoxyphenyl)-1H-pyrazole (9d). White solid; yield: 46%; ^1H NMR (500 MHz, CDCl₃) δ 8.06 (s, 1H), 7.95 (s, 1H), 7.46 (d, J = 8.0 Hz, 2H), 7.21 (d, J = 7.9 Hz, 2H), 6.95 (s, 2H), 3.95 (s, 6H), 3.88 (s, 3H), 2.38 (s, 3H); ^{13}C NMR (125 MHz, CDCl₃) δ 153.77 (2C), 138.52, 136.74, 136.63, 136.25, 129.61 (2C), 129.02, 125.59 (2C), 124.85, 123.28, 97.06 (2C), 61.04, 56.34 (2C), 21.15; HRMS calcd for $C_{19}H_{21}N_2O_3$ $[M+H]^+$ 325.1552, found 325.1551.

4.1.3.5. 4-(3,4-dimethylphenyl)-1-(3,4,5-trimethoxyphenyl)-1H-pyrazole (9e). White solid; yield: 58%; ^1H NMR (500 MHz, CDCl₃) δ 8.06 (s, 1H), 7.95 (s, 1H), 7.34 (s, 1H), 7.30 (dd, J = 7.7, 1.6 Hz, 1H), 7.16 (d, J = 7.7 Hz, 1H), 6.95 (s, 2H), 3.95 (s, 6H), 3.88 (s, 3H), 2.32 (s, 3H), 2.29 (s, 3H); ^{13}C NMR (125 MHz, CDCl₃) δ 153.77 (2C), 138.55, 137.09, 136.70, 136.27, 135.32, 130.16, 129.42, 126.96, 124.92, 123.23, 123.10, 97.02 (2C), 61.03, 56.34 (2C), 19.84, 19.46; HRMS calcd for $C_{20}H_{23}N_2O_3$ $[M+H]^+$ 339.1709, found 339.1710.

4.1.3.6. 4-(2-methoxyphenyl)-1-(3,4,5-trimethoxyphenyl)-1H-pyrazole (9f). White solid; yield: 81%; ^{1}H NMR (500 MHz, CDCl$_3$) δ 8.29 (s, 1H), 8.10 (s, 1H), 7.59 (dd, J = 7.6, 1.6 Hz, 1H), 7.26 (dd, J = 11.9, 5.4 Hz, 1H), 7.01 (dd, J = 15.1, 7.8 Hz, 2H), 6.96 (s, 2H), 3.95 (s, 6H), 3.95 (s, 3H), 3.88 (s, 3H); ^{13}C NMR (125 MHz, CDCl$_3$) δ 155.93, 153.74 (2C), 140.05, 136.78, 136.71, 136.42, 132.82, 127.79, 127.65, 126.02, 120.93, 111.37, 97.35 (2C), 61.03, 56.38 (2C), 55.49; HRMS calcd for C$_{19}$H$_{21}$N$_2$O$_4$ [M + H]$^+$ 341.1501, found 341.1498.

4.1.3.7. 4-(3-methoxyphenyl)-1-(3,4,5-trimethoxyphenyl)-1H-pyrazole (9g). White solid; yield: 96%; ^{1}H NMR (500 MHz, CDCl$_3$) δ 8.08 (s, 1H), 7.96 (s, 1H), 7.32 (t, J = 7.9 Hz, 1H), 7.15 (d, J = 7.6 Hz, 1H), 7.11–7.07 (m, 1H), 6.94 (s, 2H), 6.83 (dd, J = 8.0, 2.2 Hz, 1H), 3.94 (s, 6H), 3.88 (s, 3H), 3.86 (s, 3H); ^{13}C NMR (125 MHz, CDCl$_3$) δ 160.08, 153.78 (2C), 138.64, 136.82, 136.16, 133.31, 129.98, 124.74, 123.72, 118.23, 112.04, 111.62, 97.11 (2C), 61.03, 56.34 (2C), 55.30; HRMS calcd for C$_{19}$H$_{21}$N$_2$O$_4$ [M + H]$^+$ 341.1501, found 341.1498.

4.1.3.8. 4-(4-methoxyphenyl)-1-(3,4,5-trimethoxyphenyl)-1H-pyrazole(9h). White solid; yield: 58%; ^{1}H NMR (500 MHz, CDCl$_3$) δ 8.06 (s, 1H), 7.95 (s, 1H), 7.46 (d, J = 8.0 Hz, 2H), 7.21 (d, J = 7.9 Hz, 2H), 6.95 (s, 2H), 3.95 (s, 6H), 3.88 (s, 3H), 2.38 (s, 3H); ^{13}C NMR (125 MHz, CDCl$_3$) δ 153.77 (2C), 138.52, 136.74, 136.63, 136.25, 129.61 (2C), 129.02, 125.59 (2C), 124.85, 123.28, 97.06 (2C), 61.04, 56.34 (2C), 21.15; HRMS calcd for C$_{19}$H$_{21}$N$_2$O$_4$ [M + H]$^+$ 341.1501, found 341.1498.

4.1.3.9. 2-methoxy-5-(1-(3,4,5-trimethoxyphenyl)-1H-pyrazol-4-yl)phenol (9i). White solid; yield: 64%; ^{1}H NMR (500 MHz, CDCl$_3$) δ 8.01 (s, 1H), 7.90 (s, 1H), 7.13 (d, J = 2.0 Hz, 1H), 7.05 (dd, J = 8.3, 2.0 Hz, 1H), 6.93 (s, 2H), 6.88 (d, J = 8.3 Hz, 1H), 3.94 (s, 6H), 3.92 (s, 3H), 3.87 (s, 3H); ^{13}C NMR (125 MHz, CDCl$_3$) δ 153.76 (2C), 146.00, 145.72, 138.42, 136.71, 136.20, 125.48, 124.61, 123.20, 117.36, 112.14, 111.11, 97.04 (2C), 61.03, 56.33 (2C), 56.05; HRMS calcd for C$_{19}$H$_{21}$N$_2$O$_5$ [M + H]$^+$ 357.1450, found 357.1452.

4.1.3.10. 4-(3,4-dimethoxyphenyl)-1-(3,4,5-trimethoxyphenyl)-1H-pyrazole (9j). White solid; yield:47%; ^{1}H NMR (500 MHz, CDCl$_3$) δ 8.02 (s, 1H), 7.91 (s, 1H), 7.11 (dd, J = 8.2, 2.0 Hz, 1H), 7.04 (d, J = 2.0 Hz, 1H), 6.94 (s, 2H), 6.91 (d, J = 8.3 Hz, 1H), 3.95 (s, 3H), 3.94 (s, 6H), 3.91 (s, 3H), 3.87 (s, 3H); ^{13}C NMR (125 MHz, CDCl$_3$) δ 153.78 (2C), 149.34, 148.26, 138.45, 136.76, 136.23, 124.96, 124.83, 123.14, 118.19, 111.72, 109.32, 97.09 (2C), 61.03, 56.36 (2C), 56.02, 56.00; HRMS calcd for C$_{20}$H$_{23}$N$_2$O$_5$ [M + H]$^+$ 371.1607, found 371.1608.

4.1.3.11. 4-(4-ethoxyphenyl)-1-(3,4,5-trimethoxyphenyl)-1H-pyrazole (9k). White solid; yield: 70%; ^{1}H NMR (500 MHz, CDCl$_3$) δ 8.02 (s, 1H), 7.91 (s, 1H), 7.47 (d, J = 8.7 Hz, 2H), 6.94 (t, J = 4.3 Hz, 4H), 4.07 (q, J = 7.0 Hz, 2H), 3.95 (s, 6H), 3.88 (s, 3H), 1.44 (t, J = 7.0 Hz, 3H); ^{13}C NMR (125 MHz, CDCl$_3$) δ 158.06, 153.77 (2C), 138.38, 136.68, 136.28, 126.86 (2C), 124.68, 124.42, 122.92, 114.95 (2C), 97.00 (2C), 63.53, 61.03, 56.33 (2C), 14.84; HRMS calcd for C$_{20}$H$_{23}$N$_2$O$_4$ [M + H]$^+$ 355.1658, found 355.1655.

4.1.3.12. 4-(1-(3,4,5-trimethoxyphenyl)-1H-pyrazol-4-yl)phenol (9l). Yellow solid; yield: 77%; ^{1}H NMR (500 MHz, CDCl$_3$) δ 8.01 (s, 1H), 7.91 (s, 1H), 7.44 (d, J = 7.8 Hz, 2H), 6.94 (s, 2H), 6.88 (d, J = 7.8 Hz, 2H), 3.94 (s, 6H), 3.88 (s, 3H); ^{13}C NMR (125 MHz, CDCl$_3$) δ 154.77, 153.78 (2C), 138.35, 136.73, 136.22, 127.10 (2C), 124.65, 124.61, 123.03, 115.86 (2C), 97.07 (2C), 61.04, 56.34 (2C); HRMS calcd for C$_{18}$H$_{19}$N$_2$O$_4$ [M + H]$^+$ 327.1345, found 327.1341.

4.1.3.13. 4-(4-fluorophenyl)-1-(3,4,5-trimethoxyphenyl)-1H-pyrazole (9m). White solid; yield: 80%; ^{1}H NMR (500 MHz, CDCl$_3$) δ 8.04 (s, 1H), 7.92 (s, 1H), 7.51 (dd, J = 8.8, 5.3 Hz, 2H), 7.09 (t, J = 8.7 Hz, 2H), 6.94 (s, 2H), 3.94 (s, 6H), 3.88 (s, 3H); ^{13}C NMR (125 MHz, CDCl$_3$) δ 161.87 (d, J = 246.0 Hz), 153.80 (2C), 138.42, 136.86, 136.12, 128.12 (d, J = 3.3 Hz), 127.26 (d, J = 8.0 Hz, 2C), 123.97, 123.44, 115.85 (d, J = 21.6 Hz, 2C), 97.11 (2C), 61.03, 56.34 (2C); HRMS calcd for C$_{18}$H$_{18}$FN$_2$O$_3$ [M + H]$^+$ 329.1301, found 329.1302.

4.1.3.14. 4-(4-chlorophenyl)-1-(3,4,5-trimethoxyphenyl)-1H-pyrazole (9n). White solid; yield: 74%; ^{1}H NMR (500 MHz, CDCl$_3$) δ 8.07 (s, 1H), 7.94 (s, 1H), 7.49 (d, J = 8.5 Hz, 2H), 7.37 (d, J = 8.5 Hz, 2H), 6.93 (s, 2H), 3.94 (s, 6H), 3.88 (s, 3H); ^{13}C NMR (125 MHz, CDCl$_3$) δ 153.81 (2C), 138.42, 136.93, 136.05, 132.52, 130.48 (2C), 129.09 (2C), 126.88, 123.75, 123.63, 97.16 (2C), 61.04, 56.35 (2C); HRMS calcd for C$_{18}$H$_{18}$ClN$_2$O$_3$ [M + H]$^+$ 345.1006, found 345.1003.

4.1.3.15. 4-(4-nitrophenyl)-1-(3,4,5-trimethoxyphenyl)-1H-pyrazole (9o). Yellow solid; yield:58%; ^{1}H NMR (500 MHz, CDCl$_3$) δ 8.27 (s, 1H), 8.25 (s, 1H), 8.22 (s, 1H), 8.05 (s, 1H), 7.70 (d, J = 8.9 Hz, 2H), 6.95 (s, 2H), 3.95 (s, 6H), 3.89 (s, 3H); ^{13}C NMR (125 MHz, CDCl$_3$) δ 153.88 (2C), 146.33, 138.76, 138.69, 137.30, 135.71, 125.80 (2C), 124.74, 124.49 (2C), 122.73, 97.38 (2C), 61.06, 56.40 (2C); HRMS calcd for C$_{18}$H$_{18}$N$_3$O$_5$ [M + H]$^+$ 356.1246, found 356.1244.

4.1.3.16. 4-(thiophen-3-yl)-1-(3,4,5-trimethoxyphenyl)-1H-pyrazole (9p). Yellow solid; yield: 98%; ^{1}H NMR (500 MHz, CDCl$_3$) δ 8.02 (s, 1H), 7.89 (s, 1H), 7.38 (dd, J = 4.9, 2.9 Hz, 1H), 7.34 (dd, J = 2.9, 1.2 Hz, 1H), 7.28 (dd, J = 4.9, 1.3 Hz, 1H), 6.93 (s, 2H), 3.94 (s, 6H), 3.87 (s, 3H); ^{13}C NMR (125 MHz, CDCl$_3$) δ 153.78 (2C), 138.86, 136.78, 136.15, 132.69, 126.29, 126.07, 123.56, 120.22, 118.95, 97.08 (2C), 61.03, 56.34 (2C); HRMS calcd for C$_{16}$H$_{17}$N$_2$O$_3$S [M + H]$^+$ 317.0960, found 317.0958.

4.1.3.17. 3-(1-(3,4,5-trimethoxyphenyl)-1H-pyrazol-4-yl)pyridine (9q). White solid; yield: 91%; ^{1}H NMR (500 MHz, CDCl$_3$) δ 8.15 (s, 1H), 7.99 (s, 1H), 7.84 (d, J = 7.8 Hz, 1H), 7.69–7.63 (m, 1H), 7.56–7.51 (m, 1H), 7.45 (td, J = 7.5, 2.5 Hz, 1H), 6.95 (s, 2H), 3.94 (s, 6H), 3.87 (s, 3H); ^{13}C NMR (125 MHz, CDCl$_3$) δ 153.83 (2C), 147.84, 146.88, 138.43, 137.07, 135.93, 132.84, 132.02, 128.51, 123.93, 121.33, 97.27 (2C), 61.03, 56.37 (2C); HRMS calcd for C$_{17}$H$_{18}$N$_3$O$_3$ [M + H]$^+$ 312.1348, found 312.1345.

4.1.3.18. 4-(1-(3,4,5-trimethoxyphenyl)-1H-pyrazol-4-yl)pyridine (9r). White solid; yield: 68%; ^{1}H NMR (500 MHz, CDCl$_3$) δ 8.63 (s, 2H), 8.22 (s, 1H), 8.05 (s, 1H), 7.46 (s, 2H), 6.94 (s, 2H), 3.94 (s, 6H), 3.88 (s, 3H); ^{13}C NMR

(125 MHz, CDCl$_3$) δ 153.85 (2C), 150.21, 139.64 (2C), 138.64, 137.24, 135.77, 124.75 (2C), 122.11, 120.19, 97.37 (2C), 61.04, 56.38 (2C); HRMS calcd for C$_{17}$H$_{18}$N$_3$O$_3$ [M + H]$^+$ 312.1348, found 312.1344.

4.1.3.19. 4-(1-(3,4,5-trimethoxyphenyl)-1H-pyrazol-4-yl)-1H-indole (9s). White solid; yield: 64%; ^{1}H NMR (500 MHz, CDCl$_3$) δ 8.48 (s, 1H), 8.23 (s, 1H), 8.15 (s, 1H), 7.37 (d, $J = 7.9$ Hz, 1H), 7.29 (s, 2H), 7.25 (dd, $J = 8.9$, 4.2 Hz, 1H), 7.00 (s, 2H), 6.81 (d, $J = 0.9$ Hz, 1H), 3.96 (s, 6H), 3.90 (s, 3H); ^{13}C NMR (125 MHz, CDCl$_3$) δ 153.80 (2C), 140.01 (2C), 136.73, 136.36, 125.50, 124.73, 124.60, 124.42, 124.31, 122.31, 118.42, 110.07, 101.76, 97.21 (2C), 61.06, 56.36 (2C); HRMS calcd for C$_{20}$H$_{20}$N$_3$O$_3$ [M + H]$^+$ 350.1505, found 350.1501.

4.1.3.20. 4-(naphthalen-2-yl)-1-(3,4,5-trimethoxyphenyl)-1H-pyrazole (9t). White solid; yield: 71%; ^{1}H NMR (500 MHz, CDCl$_3$) δ 8.22 (s, 1H), 8.11 (s, 1H), 8.01 (s, 1H), 7.90–7.81 (m, 3H), 7.69 (dd, $J = 8.4$, 1.7 Hz, 1H), 7.48 (dtd, $J = 16.1$, 6.9, 1.3 Hz, 2H), 6.99 (s, 2H), 3.96 (s, 6H), 3.90 (s, 3H); ^{13}C NMR (125 MHz, CDCl$_3$) δ 153.81 (2C), 138.76, 136.85, 136.18, 133.77, 132.42, 129.31, 128.64, 127.74, 127.72, 126.47, 125.68, 124.85, 124.38, 123.83, 123.68, 97.13 (2C), 61.06, 56.37 (2C); HRMS calcd for C$_{22}$H$_{21}$N$_2$O$_3$ [M + H]$^+$ 361.1552, found 361.1550.

4.2. Biological evaluation

4.2.1. Cell culture
Human gastric adenocarcinoma SGC-7901 cells and human cervical cancer carcinoma HeLa cells were cultured in DMEM medium containing 10% fetal bovine serum, 100 U/mL streptomycins and 100 U/mL penicillin at 37 °C in a humid environment containing 5% CO$_2$. All cell lines were purchased from the American Type Culture Collection (ATCC, Manassas, VA) (Wang et al., 2021).

4.2.2. In vitro anti-proliferative activity
The in *vitro* anti-proliferative activity of CA-4 and all target compounds were determined by MTT assay (meilunbio®, China). Briefly, cells were grown into 96-well plates at a density of 5000 cells/well, depending on the growth rate of the cell line. 24 h later, cells in 96-well plates were subjected to control treatment and compound testing. After 72 h incubation at 37 °C in 5% CO$_2$, 20 μL containing MTT solution (5 mg/mL) was added to the 96-well plates. After 4 h of incubation, the culture solution containing MTT was removed and 100 mL of dimethyl sulfoxide (DMSO) was added to each well. The plates were gently stirred and incubated for 30 min at 37 °C in an incubator protected from light until the purple formazan crystals were dissolved and the OD$_{490}$ values were measured using a microplate reader. Data were calculated and plotted as percent survival compared to the control (using GraphPad Prism version 8.3.0). In the MTT assay, the half-inhibitory concentration (IC$_{50}$) was defined as the concentration of the drug that brought the absorbance to 50% of the untreated wells (Wang et al., 2016; Wang et al., 2019).

4.2.3. Effect on tubulin polymerization
The tubulin polymerization inhibition kit (Cytoskeleton-Cat. #BK011P) was used to detect the influencing factors of compound 9s on tubulin polymerization. We re-suspended tubulin in a cold G-PEM buffer (80 mM PIPES, 2 mM MgCl$_2$, 0.5 mM EGTA, 1 mM GTP, 20% (v/v) glycerol) and added it to the well of a 96-well plate containing the specified concentration of 9s or blank. The controls group were the cells treated with vehicle DMSO, the positive controls were the cells treated with CA-4, and the negative controls were the cells treated with paclitaxel. We used microplate reader (Tecan, Austria) to monitor tubulin polymerization for 61 min at 37 °C at 1 min intervals (emission wavelength: 450 nm, excitation wavelength: 360 nm) and calculated using absorbance values. Data processing was performed using GraphPad Prism 8.3.0 version (Wang et al., 2019).

4.2.4. Analysis of immunofluorescence staining
HeLa cells were inoculated in 6-well plate at a cell density of $1 \times 10^4 \sim 4 \times 10^4$ and grown for 24 h. The cells were treated for 24 h with compound 9s and CA-4 at their respective 2-fold IC$_{50}$ concentrations. The blank controls were untreated cells and the positive controls were cells treated with CA-4. Then each well was washed with PBS, which were fixed with cooled 4% formaldehyde solution for 20 min. Formaldehyde solution was discarded and 0.5% Triton-X/min was added to each well. 0.5% Triton-X was discarded and the wells were washed three times with PBST for 5 min. Added 2 mL of glycine to each well and blocked with 3% bovine serum albumin (BSA) at room temperature for 1 h. Antibody to α-microtubulin (Aclonal, China) was diluted with 3% BSA (1:100) and incubated for 3 h. The cells were washed three times with PBST solution for 10 min each to remove unbound primary antibodies. Then the FITC-coupled anti-mouse secondary antibody (1:100) and 4′,6-diamidino-2-phenylindole DAPI (1:100) were then diluted with 3% BSA and incubated for 1 h. Washed three times again with PBST for 5 min. Finally, the slices were sealed with Prolongold and photographed under a fluorescence confocal microscopy (Nikon, Japan) for a period of time (Wang et al., 2019; Liu et al., 2021).

4.2.5. Cell cycle analysis
3×10^5 Human cervical cancer cell line (HeLa) was treated with compound 9s at concentrations of 2-fold IC$_{50}$, 5-fold IC$_{50}$ and 10-fold IC$_{50}$ and the control for 24 h. Then cells were collected by centrifugation, washed with PBS, and fixed in 70% ethanol on ice. The cells were treated with Ribonuclease A (RNase) (50 mg/mL) for 30 min at 37 °C and incubated with pyridinium iodide (PI) solution (Solarbio, China) for 15 min at 4 °C. Then flow cytometry (Beckman Coulter, USA) assay was performed. We repeated these experiments at least three times (Alvarez et al., 2013).

4.2.6. Cell apoptosis assay
2×10^5 Human cervical cancer cell line (HeLa) was treated with compound 9s at concentrations of 1-fold IC$_{50}$, 2-fold IC$_{50}$ and 3-fold IC$_{50}$ for 48 h. Cells were collected using EDTA-free trypsin, centrifuged at 300r for 5 min, and the supernatant was discarded and centrifuged at 300r for 5 min at 4 °C using PBS. 100 μL of 1 × Binding Buffer was added to each sample to mix the cells. Then the cells were added with 5 μL Annexin V-FITC and 10 μL PI Staining Solution and mixed gently. After the reaction at room temperature for 15 min, 400 μL of 1 × Binding Buffer was added, mixed and

placed on ice. The samples were detected by flow cytometry (Beckman Coulter, USA) within 1 h. Apoptosis was analyzed by FlowJo_v 10.8.1 software (Huo et al., 2021; Liu et al., 2021).

4.3. Molecular modelling

The molecular modeling studies were performed with Accelrys Discovery Studio 3.0 (Dorleans et al., 2009). The crystal structure of tubulin complexed with DAMA-colchicine (PDB: 5LYJ) was retrieved from the RCSB Protein Data Bank (https://www.rcsb.org/pdb) (Wang et al., 2019).

Funding

Declaration of Competing Interest

The authors declare that they have no known competing financial interests or personal relationships that could have appeared to influence the work reported in this paper.

Appendix A. Supplementary material

Supplementary data to this article can be found online at https://doi.org/10.1016/j.arabjc.2022.104253.

References

Abdel-Aziz, M., Abuo-Rahma Gel, D., Hassan, A.A., 2009. Synthesis of novel pyrazole derivatives and evaluation of their antidepressant and anticonvulsant activities. Eur. J. Med. Chem. 44, 3480–3487. https://doi.org/10.1016/j.ejmech.2009.01.032.

Alvarez, R., Puebla, P., Diaz, J.F., et al, 2013. Endowing indole-based tubulin inhibitors with an anchor for derivatization: highly potent 3-substituted indolephenstatins and indoleisocombretastatins. J. Med. Chem. 56, 2813–2827. https://doi.org/10.1021/jm3015603.

Attard, G., Greystoke, A., Kaye, S., et al, 2006. Update on tubulin-binding agents. Pathol. Biol. (Paris) 54, 72–84. https://doi.org/10.1016/j.patbio.2005.03.003.

Beale, T.M., Allwood, D.M., Bender, A., et al, 2012. A-ring dihalogenation increases the cellular activity of combretastatin-templated tetrazoles. ACS Med. Chem. Lett. 3, 177–181. https://doi.org/10.1021/ml200149g.

Cao, Y.N., Zheng, L.L., Wang, D., et al, 2018. Recent advances in microtubule-stabilizing agents. Eur. J. Med. Chem. 143, 806–828. https://doi.org/10.1016/j.ejmech.2017.11.062.

Dorleans, A., Gigant, B., Ravelli, R.B., et al, 2009. Variations in the colchicine-binding domain provide insight into the structural switch of tubulin. Proc. Natl. Acad. Sci. USA 106, 13775–13779. https://doi.org/10.1073/pnas.0904223106.

Greene, L.M., Nathwani, S.M., Bright, S.A., et al, 2010. The vascular targeting agent combretastatin-A4 and a novel cis-Restricted {beta}-Lactam Analogue, CA-432, induce apoptosis in human chronic myeloid leukemia cells and ex vivo patient samples including those displaying multidrug resistance. J. Pharmacol. Exp. Ther. 335, 302–313. https://doi.org/10.1124/jpet.110.170415.

Hannah, J., Kelly, K., Patchett, A.A., 1975. Substituted pyrazolo corticoids as topical antiinflammatory agents. J. Med. Chem. 18, 168–172. https://doi.org/10.1021/jm00236a012.

Huo, X.S., Jian, X.E., Ou-Yang, J., et al, 2021. Discovery of highly potent tubulin polymerization inhibitors: Design, synthesis, and structure-activity relationships of novel 2,7-diaryl-[1,2,4]triazolo [1,5-a]pyrimidines. Eur. J. Med. Chem. 220, 113449. https://doi.org/10.1016/j.ejmech.2021.113449.

Johnson, M., Younglove, B., Lee, L., et al, 2007. Design, synthesis, and biological testing of pyrazoline derivatives of combretastatin-A4. Bioorg. Med. Chem. Lett. 17, 5897–5901. https://doi.org/10.1016/j.bmcl.2007.07.105.

Jordan, M.A., Wilson, L., 2004. Microtubules as a target for anticancer drugs. Nat. Rev. Cancer 4, 253–265. https://doi.org/10.1038/nrc1317.

Kucukguzel, S.G., Senkardes, S., 2015. Recent advances in bioactive pyrazoles. Eur. J. Med. Chem. 97, 786–815. https://doi.org/10.1016/j.ejmech.2014.11.059.

Kumar, S.V., Banerjee, S., Punniyamurthy, T., 2019. Rh-Catalyzed C-C/C-N bond formation via C-H activation: synthesis of 2H-indazol-2-yl-benzo a carbazoles. Org. Chem. Front. 6, 3885–3890. https://doi.org/10.1039/c9qo01120j.

Li, G., Wang, Y., Li, L., et al, 2020. Design, synthesis, and bioevaluation of pyrazolo[1,5-a]pyrimidine derivatives as tubulin polymerization inhibitors targeting the colchicine binding site with potent anticancer activities. Eur. J. Med. Chem. 202, 112519. https://doi.org/10.1016/j.ejmech.2020.112519.

Lima, L.M., Barreiro, E.J., 2005. Bioisosterism: a useful strategy for molecular modification and drug design. Curr. Med. Chem. 12, 23–49. https://doi.org/10.2174/0929867053363540.

Lin, C.M., Ho, H.H., Pettit, G.R., et al, 1989. Antimitotic natural products combretastatin A-4 and combretastatin A-2: studies on the mechanism of their inhibition of the binding of colchicine to tubulin. Biochemistry 28, 6984–6991. https://doi.org/10.1021/bi00443a031.

Liu, R., Huang, M., Zhang, S., et al, 2021. Design, synthesis and bioevaluation of 6-aryl-1-(3,4,5-trimethoxyphenyl)-1H-benzo[d]imidazoles as tubulin polymerization inhibitors. Eur. J. Med. Chem. 226, 113826. https://doi.org/10.1016/j.ejmech.2021.113826.

Loong, H.H., Yeo, W., 2014. Microtubule-targeting agents in oncology and therapeutic potential in hepatocellular carcinoma. Onco Targets Ther. 7, 575–585. https://doi.org/10.2147/OTT.S46019.

Siebert, A., Gensicka, M., Cholewinski, G., et al, 2016. Synthesis of Combretastatin A-4 Analogs and their Biological Activities. Anticancer Agents Med. Chem. 16, 942–960. https://doi.org/10.2174/1871520616666160204111832.

Tron, G.C., Pagliai, F., Del Grosso, E., et al, 2005. Synthesis and cytotoxic evaluation of combretafurazans. J. Med. Chem. 48, 3260–3268. https://doi.org/10.1021/jm049096o.

Wang, Q., Arnst, K.E., Wang, Y., et al, 2019a. Structure-Guided Design, Synthesis, and Biological Evaluation of (2-(1H-Indol-3-yl)-1H-imidazol-4-yl)(3,4,5-trimethoxyphenyl) Methanone (ABI-231) Analogues Targeting the Colchicine Binding Site in Tubulin. J. Med. Chem. 62, 6734–6750. https://doi.org/10.1021/acs.jmedchem.9b00706.

Wang, C., Yang, S., Du, J., et al, 2019b. Synthesis and bioevaluation of diarylpyrazoles as antiproliferative agents. Eur. J. Med. Chem. 171, 1–10. https://doi.org/10.1016/j.ejmech.2019.02.049.

Wang, C., Li, Y., Liu, T., et al, 2020. Design, synthesis and evaluation of antiproliferative and antitubulin activities of 5-methyl-4-aryl-3-(4-arylpiperazine-1-carbonyl)-4H-1,2,4-triazoles. Bioorg. Chem. 104, 103909. https://doi.org/10.1016/j.bioorg.2020.103909.

Wang, C., Li, Y., Liu, Z., et al, 2021a. Design, synthesis and biological evaluation of 1-Aryl-5-(4-arylpiperazine-1-carbonyl)-1H-tetrazols as novel microtubule destabilizers. J. Enzyme Inhib. Med. Chem. 36, 549–560. https://doi.org/10.1080/14756366.2020.1759582.

Wang, Z., Qi, H., Shen, Q., et al, 2016. 4,5-Diaryl-3H-1,2-dithiole-3-thiones and related compounds as combretastatin A-4/oltipraz

hybrids: Synthesis, molecular modelling and evaluation as antiproliferative agents and inhibitors of tubulin. Eur. J. Med. Chem. 122, 520–529. https://doi.org/10.1016/j.ejmech.2016.06.055.

Wang, C., Zhang, Y., Wu, Y., et al, 2021b. Developments of CRBN-based PROTACs as potential therapeutic agents. Eur. J. Med. Chem. 225, 113749. https://doi.org/10.1016/j.ejmech.2021.113749.

Wang, C., Zhang, Y., Xing, D., 2021c. Emerging Tubulin Inhibitors: A New Hope for Fungicides. J. Agric. Food Chem. 69, 11151–11153. https://doi.org/10.1021/acs.jafc.1c04048.

Wang, C., Zhang, Y., Wang, Z., et al, 2022. Design, synthesis, and biological evaluation of biotinylated colchicine derivatives as potential antitumor agents. J. Enzyme Inhib. Med. Chem. 37, 411–420. https://doi.org/10.1080/14756366.2021.2013832.

Wu, Y., Feng, D., Gao, M., et al, 2017. Design and synthesis of 5-aryl-4-(4-arylpiperazine-1-carbonyl)-2H-1,2,3-triazole derivatives as colchicine binding site inhibitors. Sci. Rep. 7, 17120. https://doi.org/10.1038/s41598-017-17449-0.

Yang, F., Jian, X.E., Diao, P.C., et al, 2020. Synthesis, and biological evaluation of 3,6-diaryl-[1,2,4]triazolo[4,3-a]pyridine analogues as new potent tubulin polymerization inhibitors. Eur. J. Med. Chem. 204, 112625. https://doi.org/10.1016/j.ejmech.2020.112625.

Zheng, S., Zhong, Q., Mottamal, M., et al, 2014. Design, synthesis, and biological evaluation of novel pyridine-bridged analogues of combretastatin-A4 as anticancer agents. J. Med. Chem. 57, 3369–3381. https://doi.org/10.1021/jm500002k.